

Supplement of Atmos. Chem. Phys., 21, 1341–1356, 2021
<https://doi.org/10.5194/acp-21-1341-2021-supplement>
© Author(s) 2021. This work is distributed under
the Creative Commons Attribution 4.0 License.



Supplement of

Measurement report: Effects of photochemical aging on the formation and evolution of summertime secondary aerosol in Beijing

Tianzeng Chen et al.

Correspondence to: Qingxin Ma (qxma@rcees.ac.cn)

The copyright of individual parts of the supplement might differ from the CC BY 4.0 License.

S1. Method for the estimation of density

The composition-dependent density of PM₁ was estimated using the following equation (Zhao et al., 2017), and the averaged density was calculated to be 1.41 g cm⁻³ (1.24-1.56 g cm⁻³, Fig. S2). This could be comparable with the density of atmospheric aerosols (1.2-1.5 g cm⁻³) determined in the Los Angeles Basin (Turpin and Lim, 2001; Geller et al., 2006) and also close to the recommended value of organic aerosol (1.4 g cm⁻³) (McMurry et al., 2002; Robert et al., 2007a; Robert et al., 2007b).

$$\rho_{\text{comp}} = \frac{[\text{NO}_3^-] + [\text{SO}_4^{2-}] + [\text{NH}_4^+] + [\text{Cl}^-] + [\text{Org}]}{\frac{[\text{NO}_3^-] + [\text{SO}_4^{2-}] + [\text{NH}_4^+]}{1.75} + \frac{[\text{Cl}^-]}{1.52} + \frac{[\text{Org}]}{1.2}}$$

where the densities are 1.75 g cm⁻³ for NH₄NO₃ and (NH₄)₂SO₄, 1.52 g cm⁻³ for NH₄Cl, and 1.2 g cm⁻³ for OA.

S2. PMF solutions and quality assurance

We carefully evaluated the PMF results and solution according to the procedures mentioned by Zhang et al. (2011) (Zhang et al., 2011) and Ulbrich et al. (2009) (Ulbrich et al., 2009). We determined the optimal solution of each dataset via examining their residuals of PMF fits (Fig. S3). When the number of factors increased from two to five, the value of Q/Q_{exp} was 2.038, 1.834, 1.736 and 1.699, respectively (Fig. S3i). As suggested by Ulbrich et al. (2009), a large decrease in Q/Q_{exp} indicates that the additional factor may explain a large fraction of unaccounted variability in the data. Meanwhile, the explained fraction of the data variation increased from 97.8 % to 99.6 % with the number of factors increased from two to five (Fig. S3i).

In order to evaluate the credibility of current PMF solution, the correlations of all factors with the corresponding reference was also obtained, which all had higher R² (>0.6), as shown in Fig. S4.

Meanwhile, we compared the mass spectra of LO-OOA with the published spectra observed in Beijing (Chen et al., 2020; Hu et al., 2016), as given in Fig. S4, and they are highly correlated with a large $R^2 > 0.8$. Meanwhile, LO-OOA and MO-OOA had the distinct diurnal variation and time series ($R^2 < 0.4$, Fig. S3c), which indicated that the identification of LO-OOA is reasonable. Based on these considerations, we concluded that the PMF solution with four factors is the optimal solutions, which exhibits the distinct time series and the corresponding mass spectrum.

S3. Back trajectories analysis

72 h back trajectories have been performed using the NOAA-HYSPLIT4 (HYbrid Single-Particle Lagrangian Integrated Trajectory) model (Draxier and Hess, 1998). Four times for each day, 00:00, 06:00, 12:00 and 18:00 UTC, terminating in a height of 50 m, and 112 trajectories were calculated and used to do the air mass cluster analysis. A total of 4 backward-trajectory clusters were identified (Clusters 1-4, Fig. S5), which indicated that more than half (Cluster 2, 64%) of the observation period is dominated by the southern air mass. This observation period included by Cluster 2 was adopted to analyze the role of t_a in PM_{10} formation and evolution.

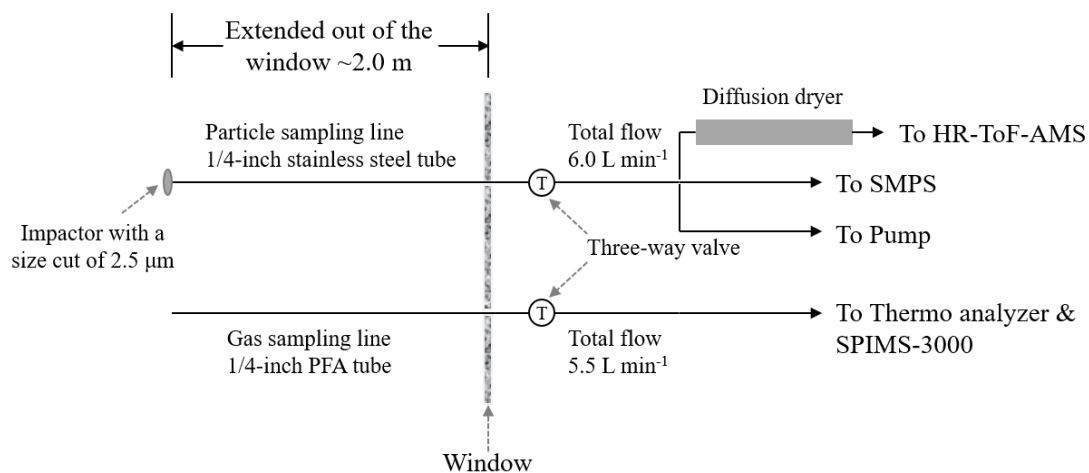


Figure S1. Detailed information of the sampling line, the corresponding flow rate, as well as the arranged instruments.

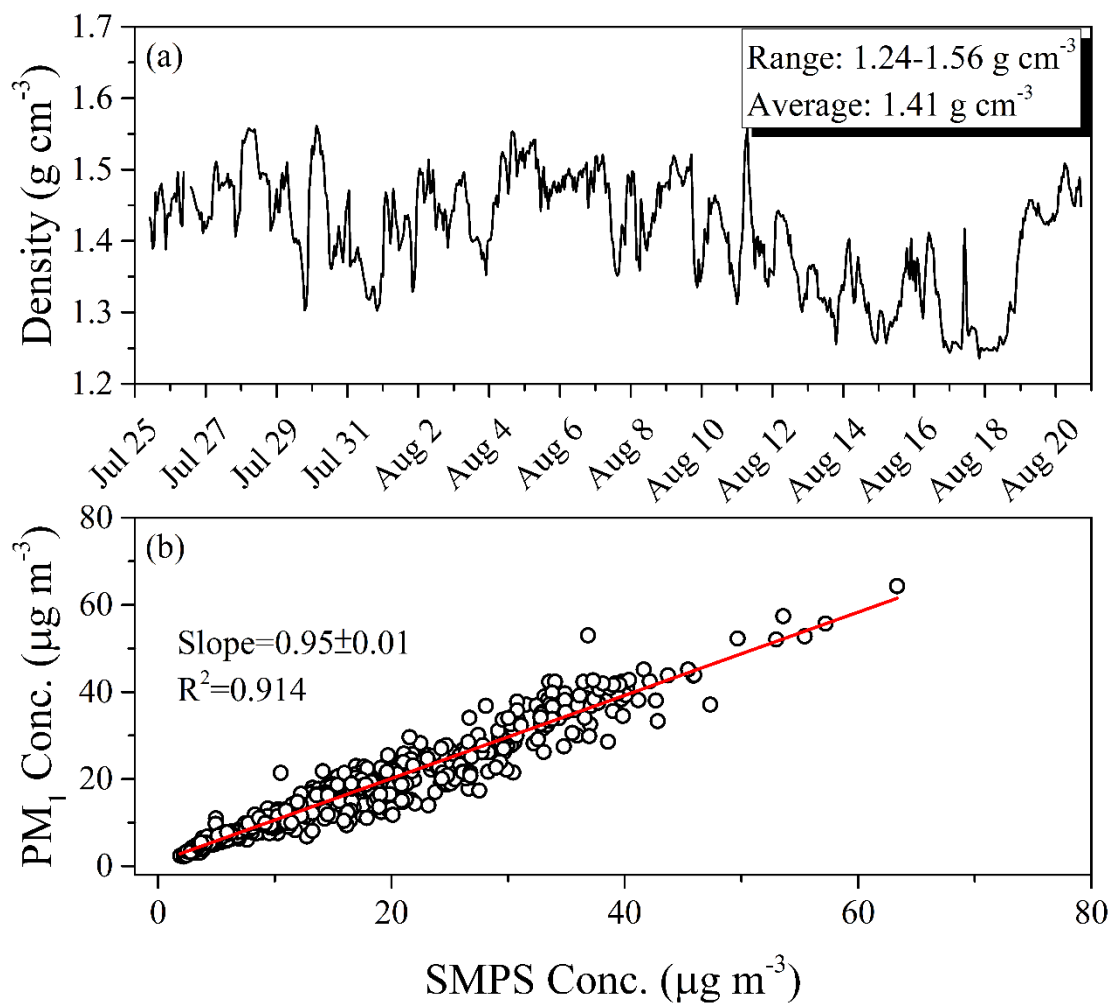


Figure S2. (a) Time series of the density of PM₁ during this field observation; (b) Relationship between PM₁ concentration derived from HR-ToF-AMS and SMPS.

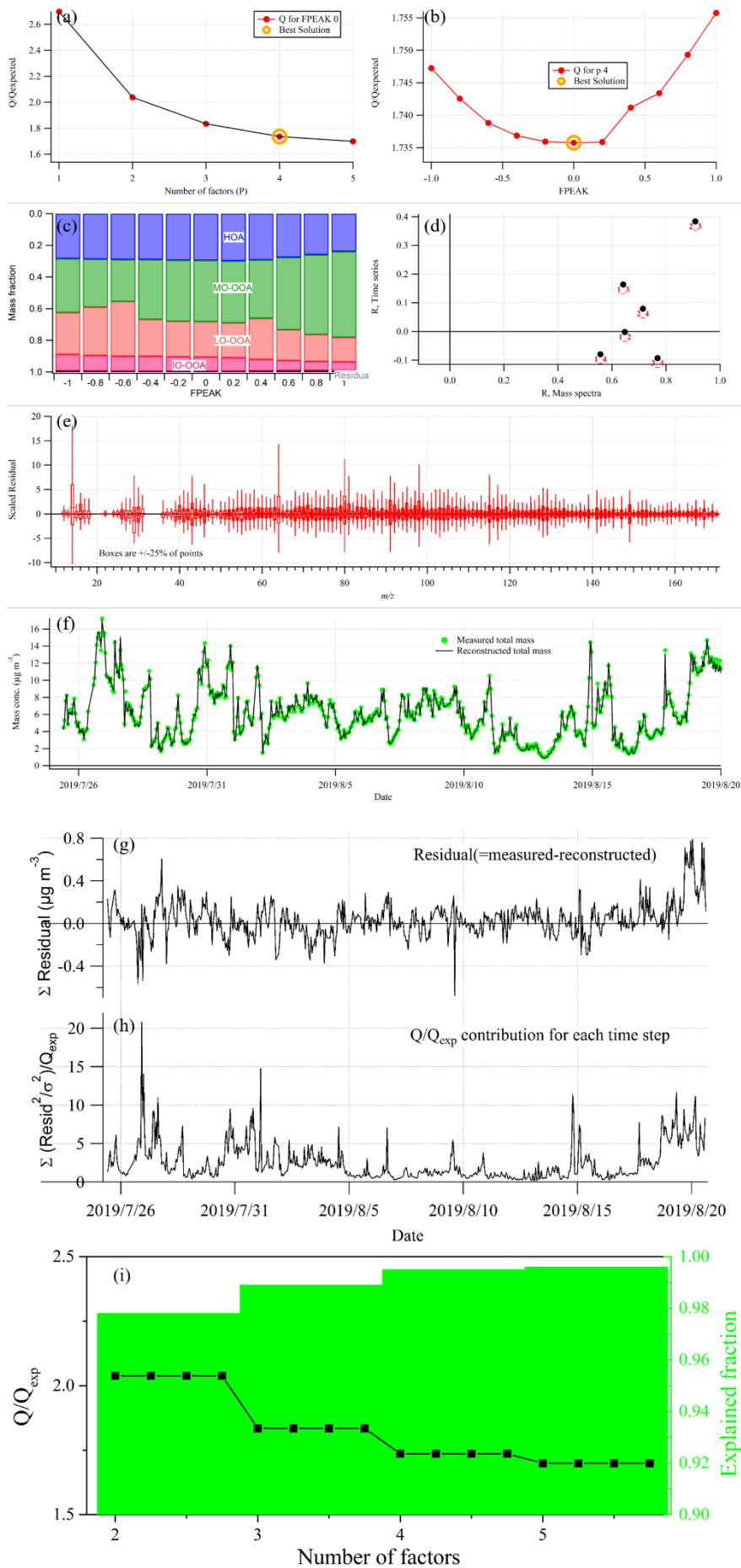


Figure S3. Summary of key diagnostic plots of the PMF results for an HR-ToF-AMS dataset acquired during this field observation: (a) Q/Q_{exp} as a function of number of factors (P) selected for PMF modeling. For the four-factor solution (i.e., the best P): (b) Q/Q_{exp} as a function of FPEAK, (c) fractions of OA factors vs. FPEAK, (d) correlations among PMF factors, (e) the box and whiskers plot showing the distributions of scaled residuals for each m/z , (f) time series of the measured organic mass and the reconstructed organic mass (= HOA + LO-OOA + IO-OOA + MO-OOA), (g) variations of the residual (= measured – reconstructed) of the fit, (h) the Q/Q_{exp} for each point in time, (i) the changes of Q/Q_{exp} and the explained variation from two-factor to five-factor solutions.

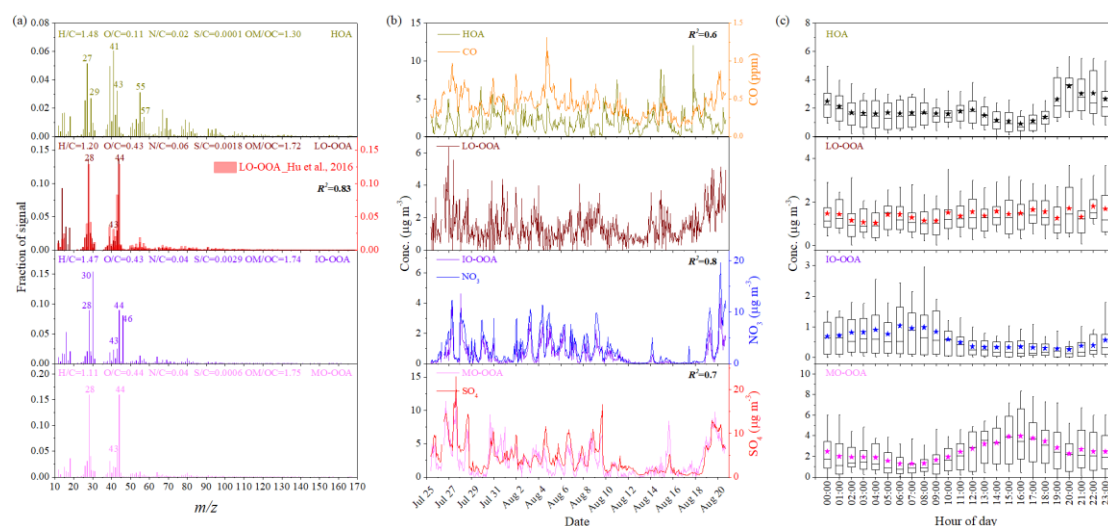


Figure S4. (a) Mass spectra, (b) time series, and (c) diurnal variation of the four factors (HOA, LO-OOA, IO-OOA and MO-OOA) identified from the PMF analysis to the HR-ToF-AMS data during the whole field observation. The upper and lower boundaries of boxes indicate the 75th and 25th percentiles; the line within the box marks the median; the whiskers above and below boxes indicate the 90th and 10th percentiles; and colored asterisk symbols represent the means.

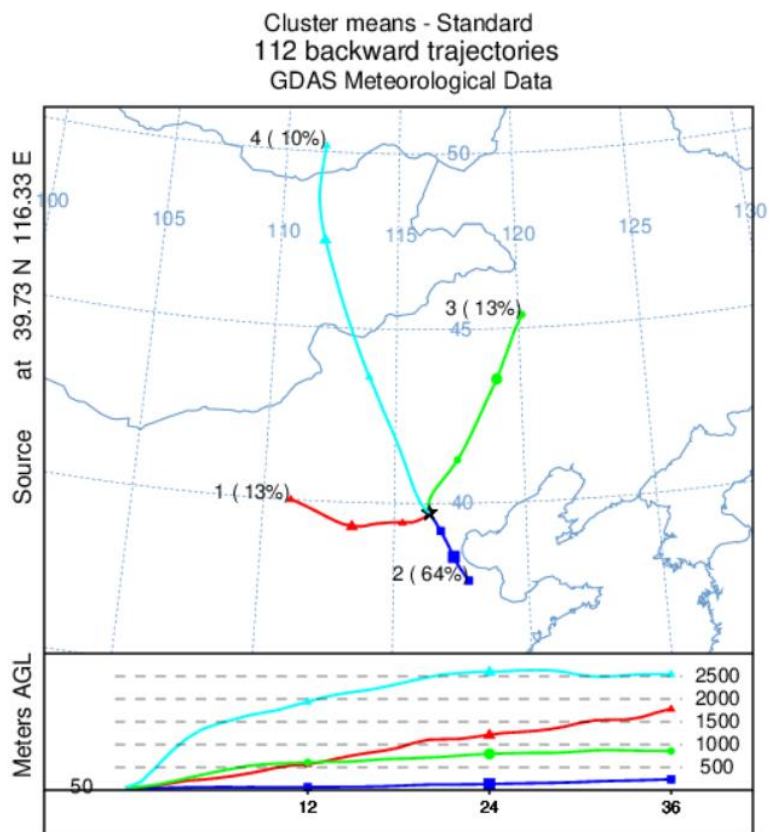


Figure S5. Mean back trajectories for 4 trajectory clusters arriving at Beijing Institute of Petrochemical Technology (BIPT) from different height.

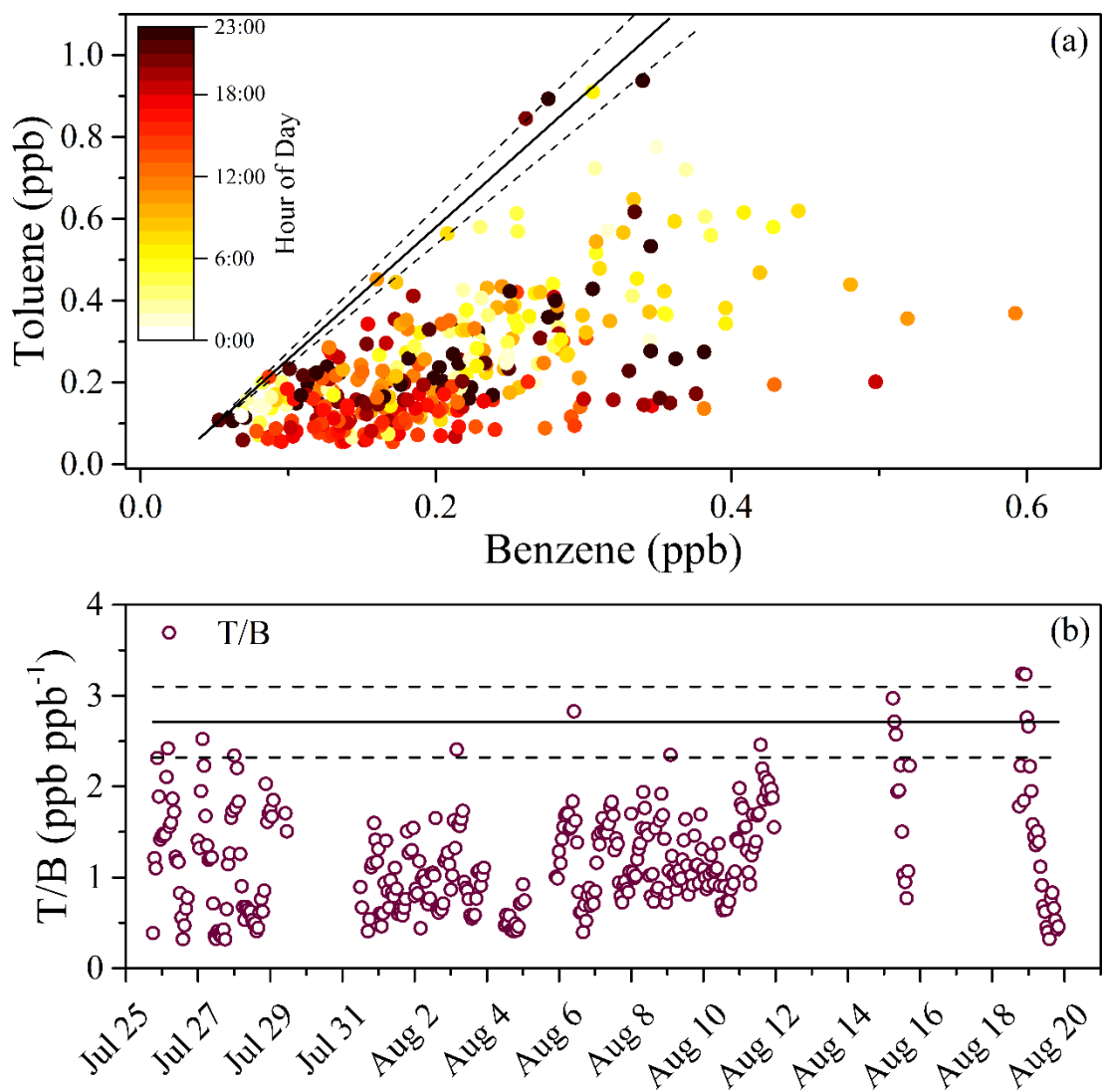


Figure S6. (a) Determination of the emission ratio of toluene vs. benzene. The scatter plot of toluene vs. benzene color-coded by the time of day, (b) Time series of concentration ratio of benzene and toluene during the observation period included by Cluster 2.

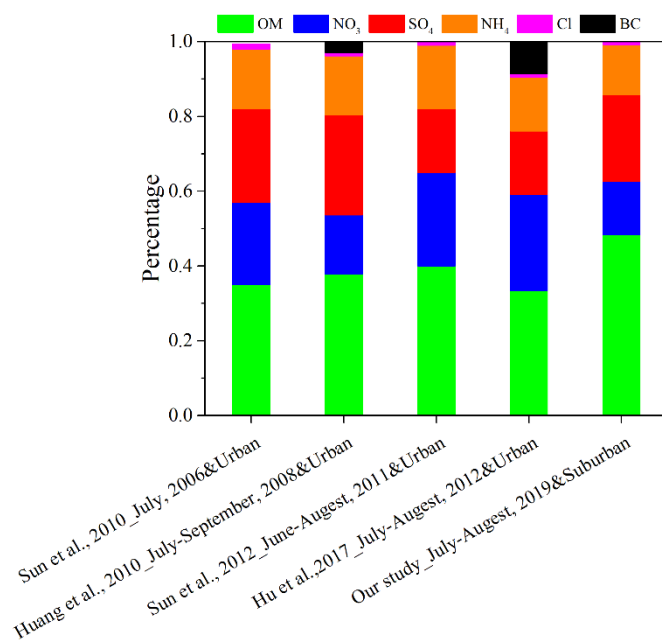


Figure S7. Comparison of percentage of different chemical species in PM₁ derived from other observations in summertime of Beijing in urban and suburban.

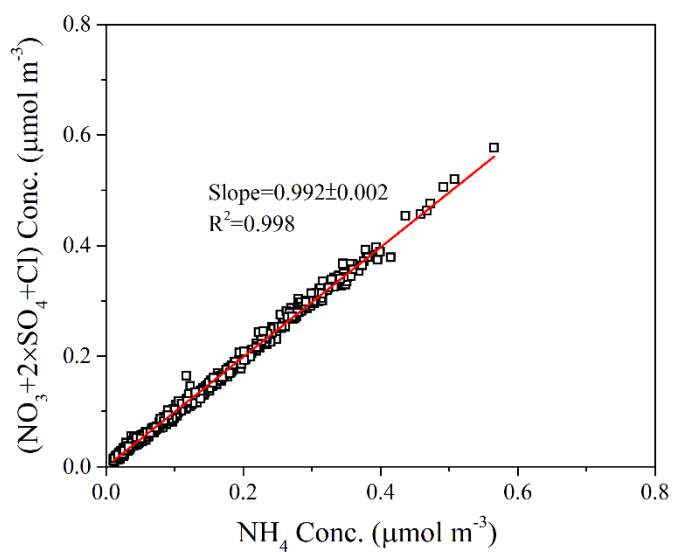


Figure S8. Linear relationship between NO₃+2×SO₄+Cl and NH₄ measured by the HR-ToF-AMS.

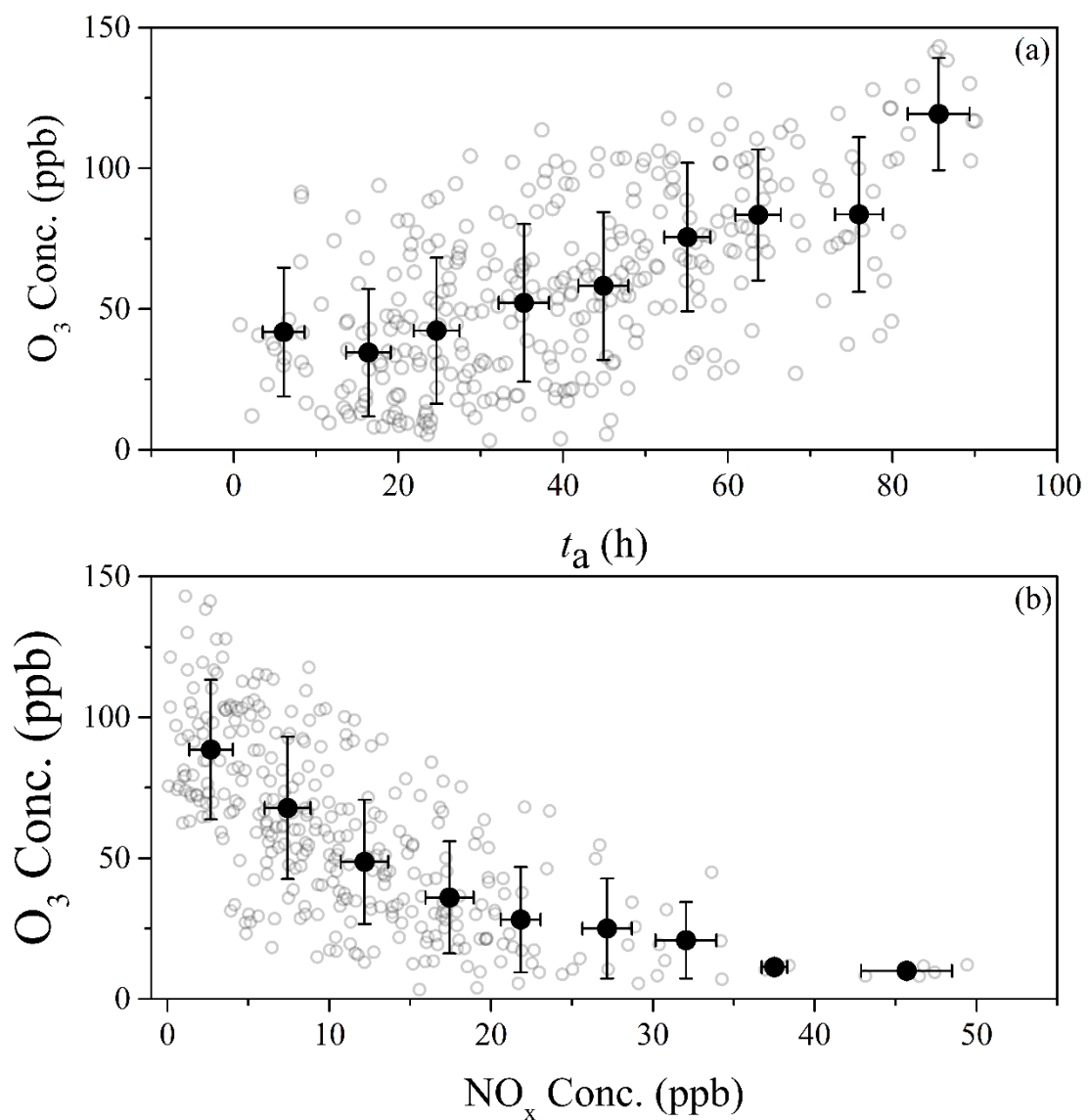


Figure S9. (a) Relationship between photochemical age (t_a) and O₃ concentration. The data are binned according to the value of t_a (10 h increment); (b) Relationship between NO_x and O₃ concentration. The data are binned according to the value of NO_x (5 ppb increment).

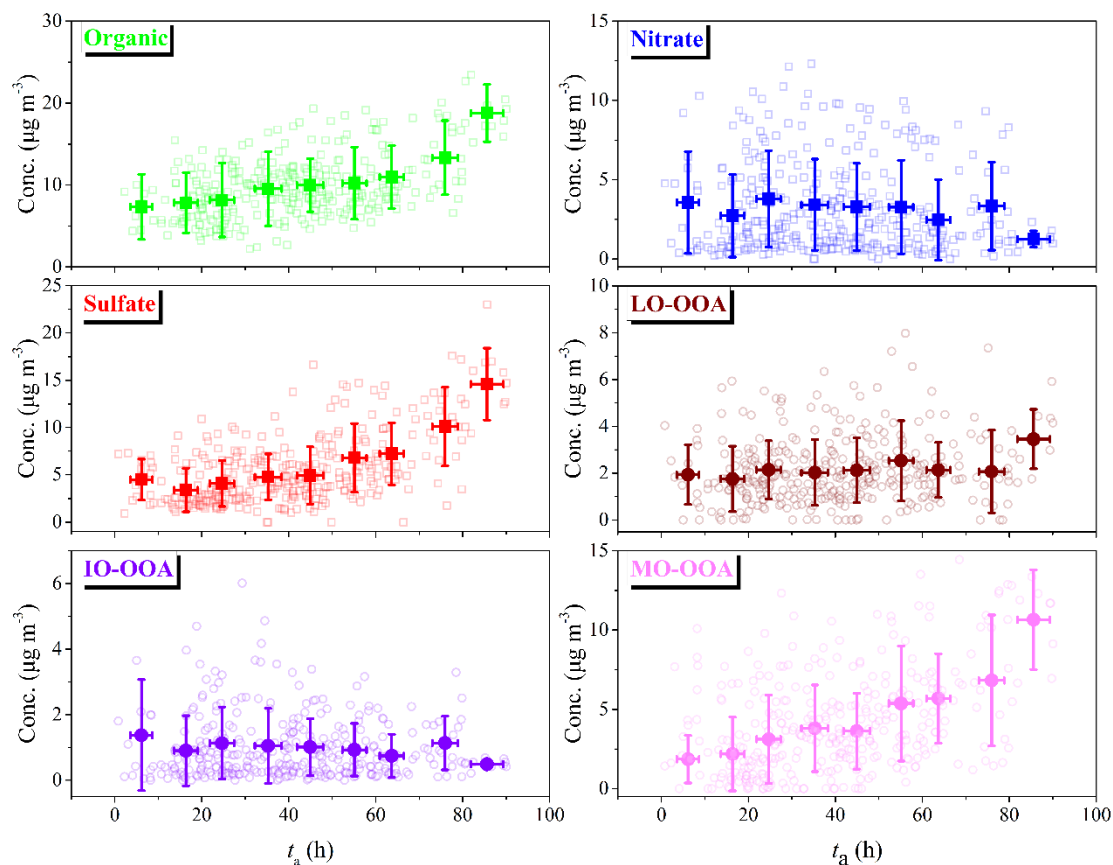


Figure S10. Variations of mass concentrations of NR-PM₁ species and OA factors as a function of t_a . The data are binned according to the value of t_a (10 h increment).

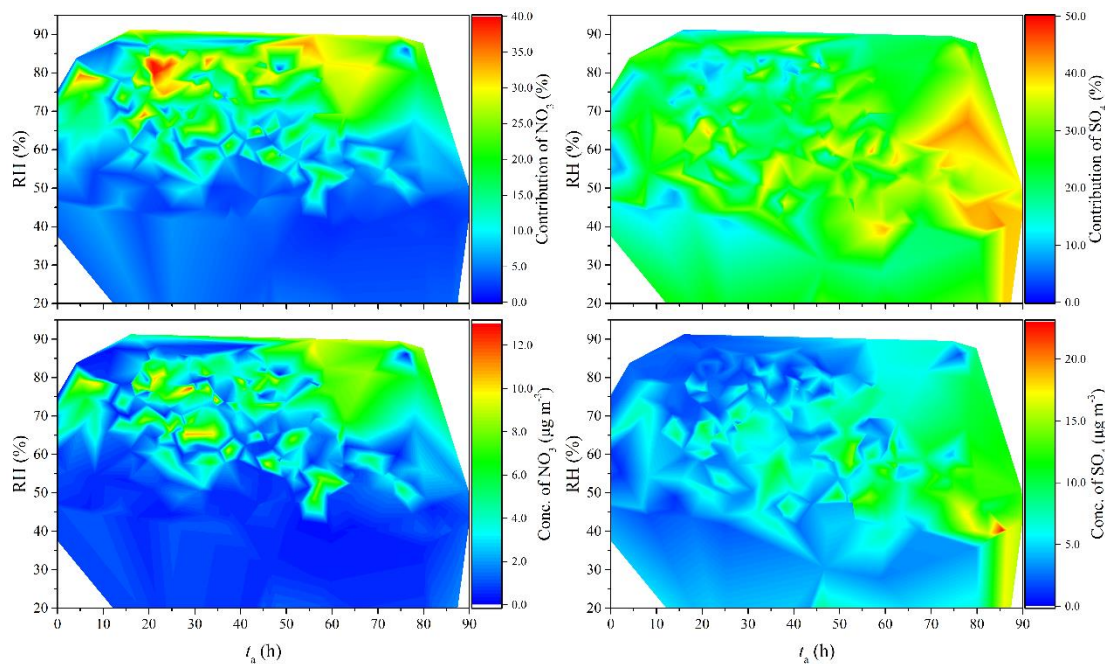


Figure S11. t_a - and RH-dependent distributions of NO₃ and SO₄ during the whole field observation.

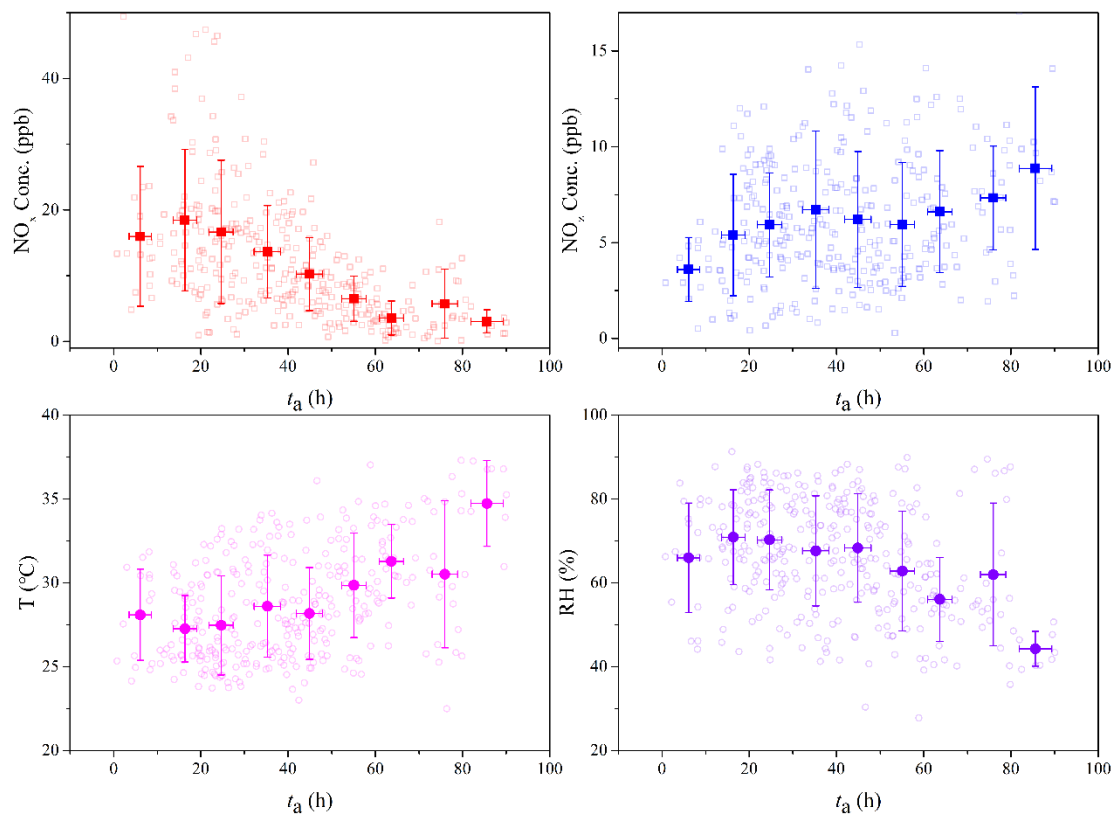


Figure S12. Variations of mass concentrations of NO_x , NO_z , and meteorological conditions (RH and T) as a function of t_a . The data are binned according to the value of t_a (10 h increment).

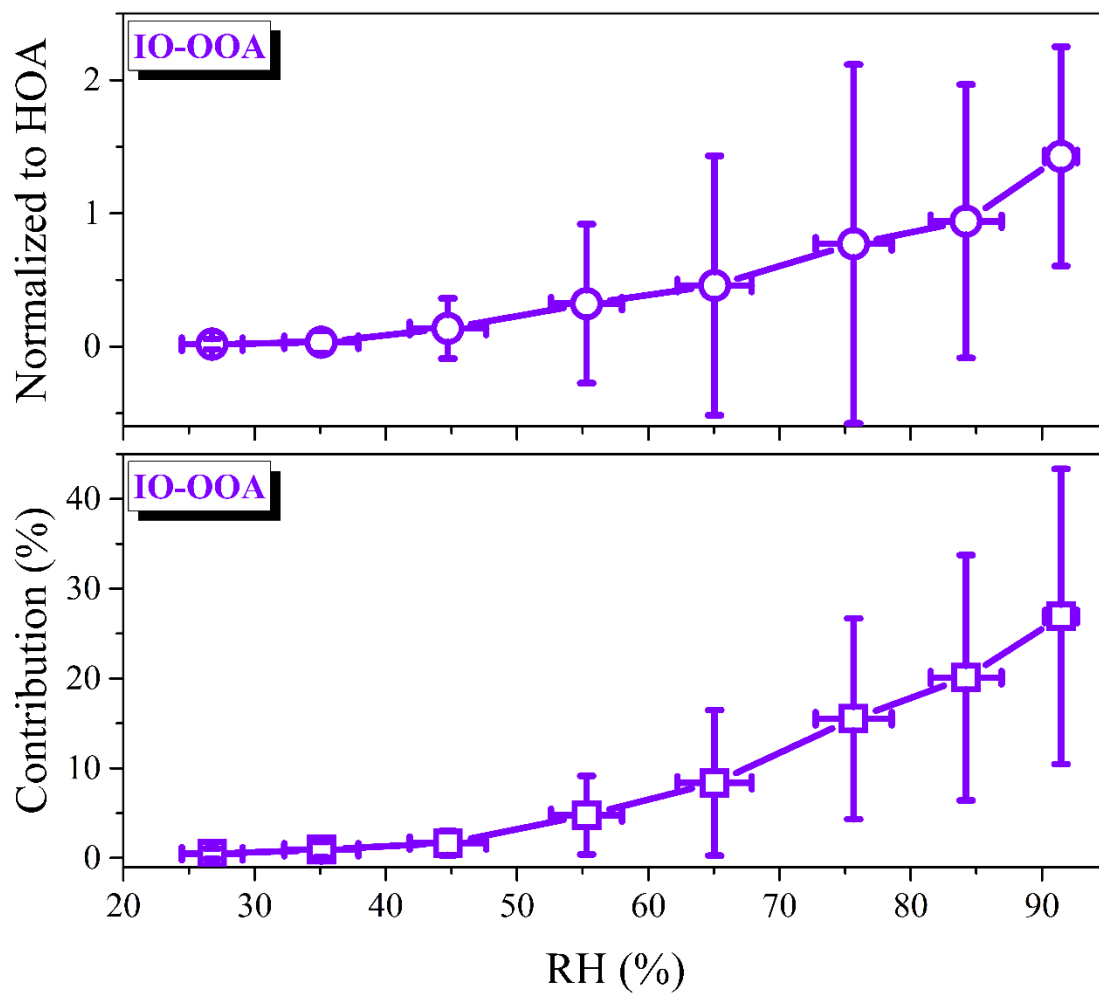


Figure S13. Variations of normalized mass concentration to HOA and contribution of IO-OOA as a function of RH. The data are binned according to RH (10 % increment).

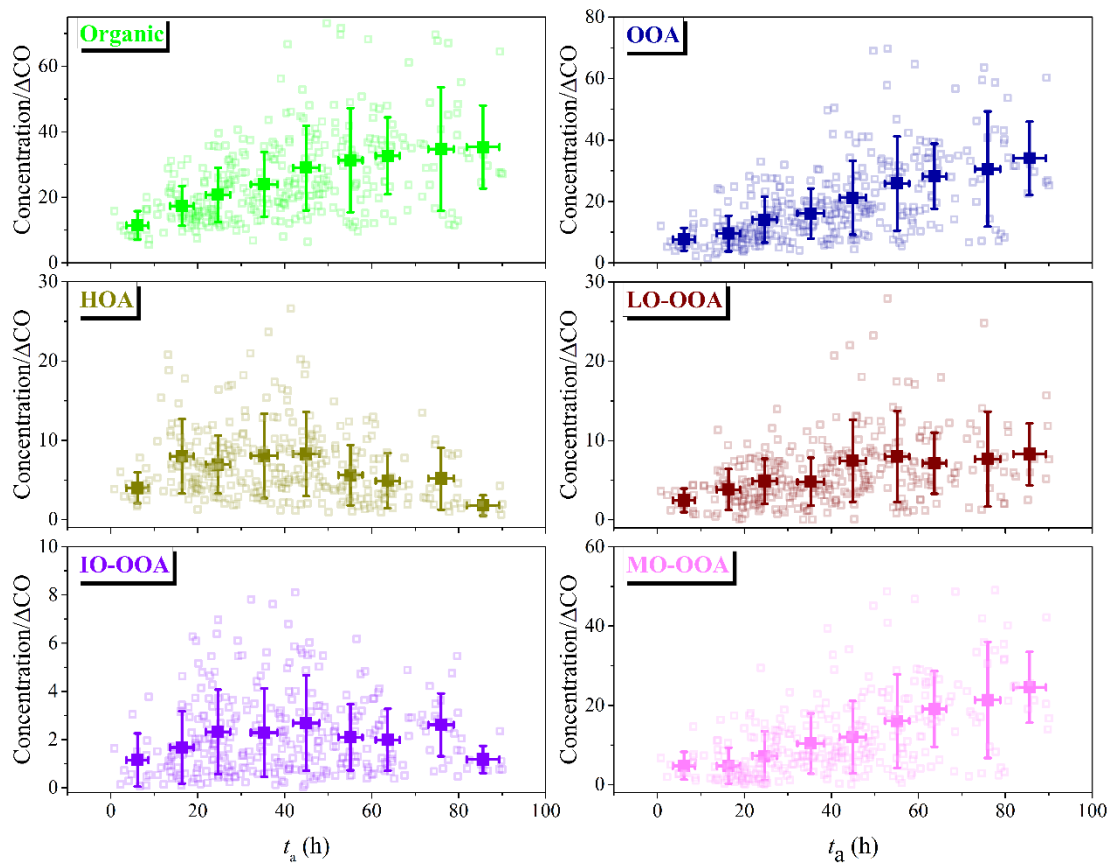


Figure S14. The evolution of OA/ Δ CO vs. photochemical age. The data are binned according to the value of t_a (10 h increment).

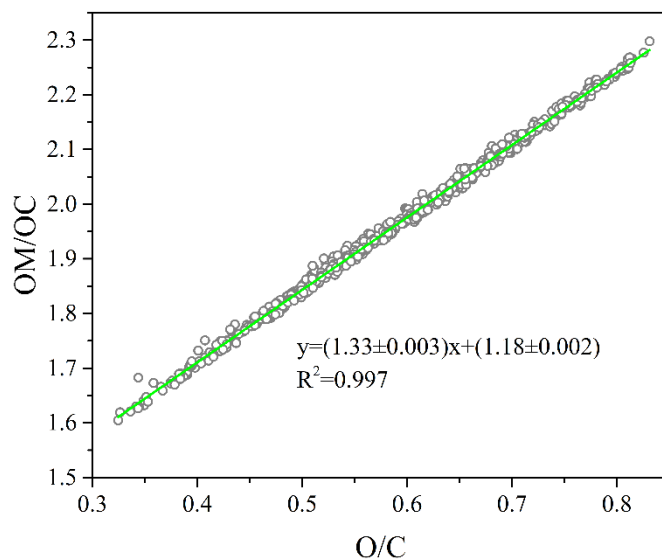


Figure S15. Relationship between OM/OC and O/C during this field observation.

References

Chen, T., Liu, J., Liu, Y., Ma, Q., Ge, Y., Zhong, C., Jiang, H., Chu, B., Zhang, P., Ma, J., Liu, P., Wang,

Y., Mu, Y., and He, H.: Chemical characterization of submicron aerosol in summertime Beijing: A case study in southern suburbs in 2018, *Chemosphere*, 247, 125918, <https://doi.org/10.1016/j.chemosphere.2020.125918>, 2020.

Draxier, R. R., and Hess, G. D.: An overview of the HYSPLIT_4 modelling system for trajectories, dispersion and deposition, *Aust. Meteorol. Mag.*, 47, 295-308, 1998.

Geller, M., Biswas, S., and Sioutas, C.: Determination of particle effective density in urban environments with a differential mobility analyzer and aerosol particle mass analyzer, *Aerosol Sci. Tech.*, 40, 709-723, [10.1080/02786820600803925](https://doi.org/10.1080/02786820600803925), 2006.

Hu, W., Hu, M., Hu, W., Jimenez, J. L., Yuan, B., Chen, W., Wang, M., Wu, Y., Chen, C., Wang, Z., Peng, J., Zeng, L., and Shao, M.: Chemical composition, sources, and aging process of submicron aerosols in Beijing: Contrast between summer and winter, *J. Geophys. Res. Atmos.*, 121, 1955-1977, [doi:10.1002/2015JD024020](https://doi.org/10.1002/2015JD024020), 2016.

McMurry, P. H., Wang, X., Park, K., and Ehara, K.: The relationship between mass and mobility for atmospheric particles: A new technique for measuring particle density, *Aerosol Sci. Tech.*, 36, 227-238, [10.1080/027868202753504083](https://doi.org/10.1080/027868202753504083), 2002.

Robert, M. A., Kleeman, M. J., and Jakober, C. A.: Size and composition distributions of particulate matter emissions: Part 2- Heavy-duty diesel vehicles, *J. Air Waste Manage.*, 57, 1429-1438, [10.3155/1047-3289.57.12.1429](https://doi.org/10.3155/1047-3289.57.12.1429), 2007a.

Robert, M. A., VanBergen, S., Kleeman, M. J., and Jakober, C. A.: Size and composition distributions of particulate matter emissions: Part 1 - Light-duty gasoline vehicles, *J. Air Waste Manage.*, 57, 1414-1428, [10.3155/1047-3289.57.12.1414](https://doi.org/10.3155/1047-3289.57.12.1414), 2007b.

Turpin, B. J., and Lim, H. J.: Species contributions to PM_{2.5} mass concentrations: Revisiting common

assumptions for estimating organic mass, *Aerosol Sci. Tech.*, 35, 602-610, 10.1080/02786820152051454, 2001.

Ulbrich, I. M., Canagaratna, M. R., Zhang, Q., Worsnop, D. R., and Jimenez, J. L.: Interpretation of organic components from positive matrix factorization of aerosol mass spectrometric data, *Atmos. Chem. Phys.*, 9, 2891-2918, 10.5194/acp-9-2891-2009, 2009.

Zhang, Q., Jimenez, J. L., Canagaratna, M. R., Ulbrich, I. M., Ng, N. L., Worsnop, D. R., and Sun, Y.: Understanding atmospheric organic aerosols via factor analysis of aerosol mass spectrometry: a review, *Anal. Bioanal. Chem.*, 401, 3045-3067, 10.1007/s00216-011-5355-y, 2011.

Zhao, J., Du, W., Zhang, Y., Wang, Q., Chen, C., Xu, W., Han, T., Wang, Y., Fu, P., Wang, Z., Li, Z., and Sun, Y.: Insights into aerosol chemistry during the 2015 China Victory Day parade: results from simultaneous measurements at ground level and 260 m in Beijing, *Atmos. Chem. Phys.*, 17, 3215-3232, 10.5194/acp-17-3215-2017, 2017.